Dalton Transactions

ROYAL SOCIETY OF CHEMISTRY

PAPER

View Article Online
View Journal | View Issue

Cite this: *Dalton Trans.*, 2022, **51**, 18520

iClick synthesis of network metallopolymers†

Yu-Hsuan Shen,[a] Ion Ghiviriga,[a] Khalil A. Abboud,[a] Kirk S. Schanze[b] and Adam S. Veige*[a]

Received 24th May 2022,
Accepted 14th November 2022

DOI: 10.1039/d2dt01624a

rsc.li/dalton

Described is an approach to preparing the first iClick network metallopolymers with porous properties. Treating digoldazido complex **2-AuN$_3$** with trigoldacetylide **3-AuPPh$_3$** or **3-AuPEt$_3$**, trialkyne **3-H**, tetragoldacetylide **4-AuPPh$_3$**, or tetraalkyne **4-H** in CH_2Cl_2 affords five iClick network metallopolymers **5-AuPPh$_3$**, **5-AuPEt$_3$**, **5-H**, **6-AuPPh$_3$**, and **6-H**. Confirmation of the iClick network metallopolymers comes from FTIR, ^{13}C solid-state cross-coupling magic angle spinning (CPMAS) NMR spectroscopy, thermogravimetric analysis (TGA), differential scanning calorimetry (DSC), and nitrogen and CO_2 sorption analysis. Employing model complexes **7-AuPPh$_3$**, **7-AuPEt$_3$**, **7-H**, **8-AuPPh$_3$**, and **8-H** provides structural insights due to the insolubility of iClick network metallopolymers.

Introduction

Heterogeneous catalysts are useful in industrial processes due to their advantageous sustainability, recyclability, robustness, and ease of catalyst/product separation.[1,2] Accessible and tunable by a simple choice of building block, porous organic polymers (POPs) have numerous applications[3–9] in catalysis,[3,10–12] medicine,[13,14] gas separation,[15,16] CO_2 capture,[17–21] and as sorbents.[22–29] POPs are highly selective catalysts and can lower process costs.[30]

A few porous polymers incorporating metal ions (metal-POP) using polypyridines,[31–33] phthalocyanine,[34,35] and porphyrins[36–41] as ligands have been synthesized. Post-polymerization metalation[31–33,42] or polymerization using monomers bearing metal centers[31,34–41] are the two methods for incorporating metal ions in porous polymers. The former approach can result in incomplete metalation, and the latter approach requires metal catalysts for polymerization[43]

In contrast to the methods incorporating metal ions, POP synthesis employs a diverse variety of chemical reactions. Yamamoto,[44–46] Sonogashira–Hagihara,[47] Suzuki–Miyaura,[48] Friedel–Crafts,[49–51] and copper(I)-catalyzed azide-alkyne cycloaddition (CuAAC),[52] are some of the reaction types utilized in POP synthesis. Related to this work, highly stable POPs with large surface areas[53,54] that employ CuAAC in their synthesis are beneficial in small molecule gas capture,[55–60] photocatalysis,[61,62] and as supports for heterogeneous catalysis.[52,63] POPs synthesized using click-based CuAAC are now relatively common in the literature. Absent however, are network polymers synthesized using inorganic click (iClick)[64] methodologies. An advantage of using iClick is the ability to directly incorporate metal ions into the polymer backbone repeating unit. Demonstrated already for linear polymers,[65–67] extension of iClick to network polymers has yet to be achieved. Finding a new route to install metal ions in POPs will broaden the application space of these materials.

iClick is a rapid, simple, and high yield reaction that is widely applicable to a variety of metals. Some of the first cycloaddition reactions involving metal ions and electron deficient alkynes were reported in the mid-1970's.[69,70] Related to this work, in 2007, Gray *et al.* demonstrated the monogold-azide (**1-AuN$_3$**) cycloaddition with alkynes according to Scheme 1A.[71–80]

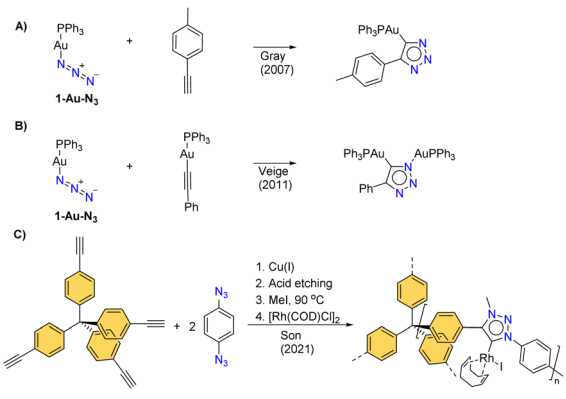

Scheme 1 (A) Early examples of gold(I) 1,2,3-triazolate complexes from cycloaddition reactions,[68] (B) bimetallic iClick reaction of gold(I) azido complex with a gold(I) acetylide,[64] (C) post-polymerization synthesis of the only metal click-based POP.[42]

[a]*University of Florida, Department of Chemistry, Center for Catalysis, P.O. Box 117200, Gainesville, FL, 32611, USA. E-mail: veige@chem.ufl.edu*
[b]*University of Texas at San Antonio, Department of Chemistry, One UTSA Circle, San Antonio, TX 78249, USA*

†Electronic supplementary information (ESI) available: Experimental details: Tables S1–S4, and Fig. S1–S53. CCDC 2158225 and 2158226. For ESI and crystallographic data in CIF or other electronic format see DOI: **https://doi.org/10.1039/d2dt01624a**

Unleashing the possibility of linking metal ions *via* cycloaddition chemistries, bimetallic complexes produced from metal-azides and metal-acetylides were published by our group in 2011 (Scheme 1B).[64,80–87] Son *et al.* reported the only example of a click-based POP that incorporates a metal ion, though the metal addition occurs *via* post-polymerization functionalization at the periphery of the backbone according to Scheme 1C.[42] Nonetheless, the Rh-POP has a surface area of 310 $m^2\ g^{-1}$ and is an active catalyst for the polymerization of arylacetylenes. Here, we present the first use of iClick to build metal containing network organometallic polymers using monomers bearing metal centers without the use of catalysts.

Results

Monomer synthesis and characterization: Au(I) complexes (2-AuN$_3$, 3-AuPEt$_3$, and 4-AuPPh$_3$)

2-AuN$_3$. Creating a network polymer using iClick requires the synthesis of several unique monomers. Needed is a digold complex that serves to link the other units in the polymer. Combining $(AuCl)_2(PPh_2(C_6H_4)PPh_2)$[88] and silver triflate in THF for 1 d followed by filtration produces $(AuOTf)_2(PPh_2(C_6H_4)PPh_2)$. Dissolving the white powder again in a mixture of THF : MeOH (3 : 1 v/v) with sodium azide for 1 d produces complex **2-AuN$_3$** in 81% isolated yield. This two-step process avoids the formation of highly explosive AgN_3.

Evidence for the structural assignment of **2-AuN$_3$** comes from NMR and IR spectroscopy, and single crystal X-ray diffraction. Attributable to the phosphorous atom, in the $^{31}P\{^1H\}$ NMR spectrum, a single resonance appears at 30.9 ppm. An absorption at 2052 cm^{-1} in the FTIR spectrum reveals the presence of the azide functionality. Single crystals suitable for X-ray crystallography deposit from a concentrated solution of **2-AuN$_3$** in CH_2Cl_2 at −25 °C. C_i-symmetric in solid state and crystallizing in the *C*2/*c* space group, X-ray data refinement reveals the dinuclear composition of **2-AuN$_3$** (Fig. 1).

3-AuPEt$_3$ and 4-AuPPh$_3$. Porous polymer synthesis requires branching points that extend from multivalent monomers. Combining $AuCl(PPh_3)$ and tetrakis(4-((trimethylsilyl)ethynyl)phenyl)methane[54] in CH_2Cl_2 for 1 d at ambient temperature yields **4-AuPPh$_3$** in 71% yield. Identifiable by NMR, IR spectroscopy, and single crystal X-ray diffraction, complex **4-AuPPh$_3$** is tetranuclear. In the $^{31}P\{^1H\}$ NMR spectrum of **4-AuPPh$_3$**, a singlet at 42.3 ppm is attributable to the phosphorous atom on the PPh_3. The acetylide carbon attached to the Au(I) ion resonates at the distinct position of 104.0 ppm in the $^{13}C\{^1H\}$ NMR spectrum. Assigned to the acetylide stretching vibration, an IR spectrum reveals an absorption at 2119 cm^{-1}. Layering a concentrated CH_2Cl_2 solution of **4-AuPPh$_3$** with pentane precipitates yellow single crystals suitable for X-ray diffraction. Fig. 2 depicts the molecular structure of **4-AuPPh$_3$**. Significant rotational disorder within the crystal structure only allows for refinement data of R_1 = 9.79%. Numerous crystallization attempts and X-ray crystallography did not provide better refinement. The rotational disorder comes from the protruding acetylide functionality combined with the presence of a triphenyl phosphine group at the end. Using a slightly modified synthesis[89] with $AuCl(PPh_3)$ and 1,3,5-tris(trimethylsilylethynyl)benzene,[90] the trivalent derivative **3-AuPEt$_3$** was also synthesized in 81% yield (Fig. S6–S10 in the ESI†).

Synthesis of iClick model complexes (7-AuPPh$_3$, 7-AuPEt$_3$, 8-AuPPh$_3$, 7-H, and 8-H)

Synthesis of model complexes. Anticipating the need for soluble model complexes, iClick reactions were designed to synthesize small molecule analogues of network polymers.

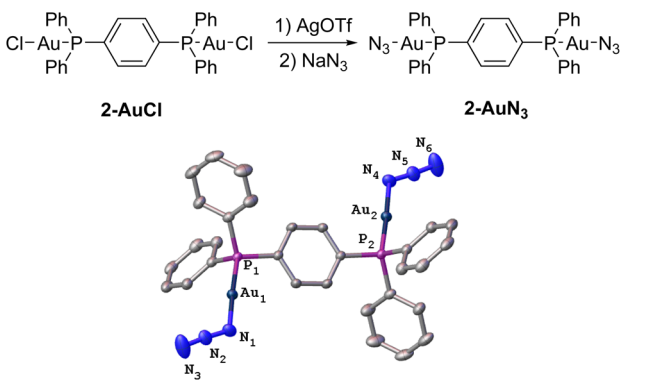

Fig. 1 Synthesis and molecular structure of **2-AuN$_3$** with ellipsoids drawn at the 50% probability level and hydrogen atoms removed for clarity.

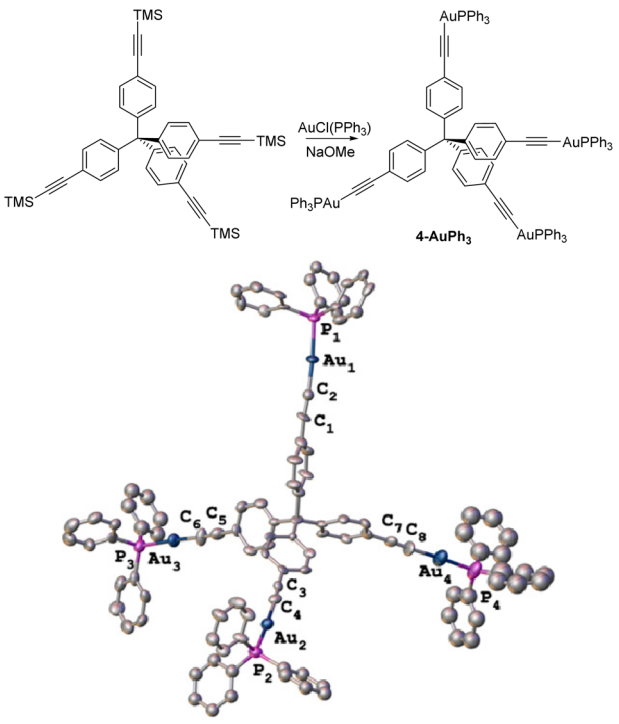

Fig. 2 Synthesis and molecular structure of **4-AuPPh$_3$** with ellipsoids drawn at the 50% probability level and hydrogen atoms removed for clarity.

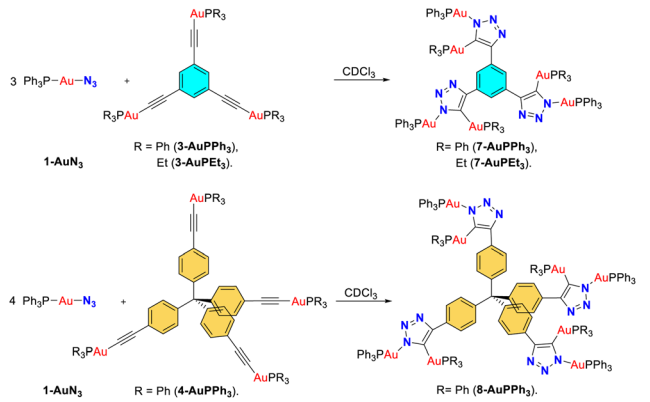

Scheme 2 Synthesis of model complexes (**7-AuPPh$_3$**, **7-AuPEt$_3$**, and **8-AuPPh$_3$**) using goldazido complex **1-AuN$_3$** with trigoldacetylide **3-AuPPh$_3$** or **3-AuPEt$_3$** and tetragoldacetylide **4-AuPPh$_3$**.

Scheme 2 depicts the iClick reaction between azidogold complex **1-AuN$_3$**[91] and gold acetylides **3-AuPPh$_3$**,[88] **3-AuPEt$_3$**, and **4-AuPPh$_3$** to form **7-AuPPh$_3$**, **7-AuPEt$_3$**, and **8-AuPPh**, respectively. Instead of a difunctional azide, a monoazide caps the ends of monomers **3-AuPPh$_3$**, **3-AuPEt$_3$**, **4-AuPPh$_3$**. Scheme 3 depicts the synthesis of analogous model complexes that employ the organic alkynes **3-H** and **4-H** in place of the Au-acetylides to produce **7-H** and **8-H**.

The iClick reaction occurs readily in $CDCl_3$ at room temperature to give the five model complexes as yellow powders. Monitoring all five reactions with ^{1}H and ^{31}P{^{1}H} NMR spectroscopy allows for *in situ* monitoring of product formation. Only temporarily soluble, mixing the azides with acetylides or alkynes eventually results in yellow solid precipitate within hours presumably due to aurophilic[82] and π–π interactions.[92] Changing the solvent and increasing the temperature both fail to solubilize the monomers. Consequently, all five model complexes were characterized *in situ* by solution-phase NMR spectroscopy.

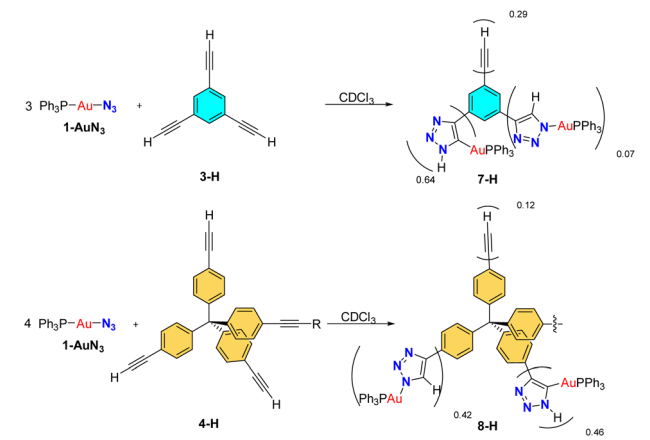

Scheme 3 Synthesis of model complexes (**7-H** and **8-H**) using goldazido complex **1-AuN$_3$** with trialkyne **3-H** and tetraalkyne **4-H**.

Monitoring the formation of complexes **7-AuPPh$_3$**, **7-AuPEt$_3$**, and **8-AuPPh$_3$** *in situ* with ^{1}H and ^{31}P{^{1}H} NMR spectroscopy reveals complete conversion of starting materials after 12 h. In the ^{31}P{^{1}H} NMR spectrum ($CDCl_3$), **7-AuPPh$_3$** exhibits two singlets at 43.7 and 30.6 ppm, while **8-AuPPh$_3$** exhibits two singlets at 44.2 and 30.8 ppm attributable to the two PPh_3 ligands. Due to extensive phosphine exchange between PEt_3 and PPh_3 the ^{31}P{^{1}H} NMR spectrum of **7-AuPEt$_3$** exhibits numerous signals and precludes an absolute assignment.

Complex **7-H** presents two singlets at 43.3 and 29.9 ppm, while **8-H** exhibits signals at 43.3 and 29.0 ppm in the ^{31}P{^{1}H} NMR spectra (Scheme 3). The downfield signal in the ^{31}P{^{1}H} NMR spectra corresponds the N-Au-*P* and the upfield signal is attributable to the C-Au-*P* phosphorous. The presence of the upfield signal is clear evidence that the Au(I) fragment migrates from the triazolate N-atom to the C-atom. Eqn (1) depicts the Au migration. Thus, **7-H** and **8-H** are mixtures of the two C-bound and N-bound derivatives. Previous examples of this rapid isomerization with terminal alkynes in iClick chemistry have been reported extensively.[75,82] More evidence for the isomerization comes from the ^{1}H NMR spectra of both complexes. Indicatives of a proton migration from the carbon atom to the nitrogen of the triazolate ring, complex **7-H** and **8-H** exhibit singlets at 11.85 and 11.66 ppm, respectively.

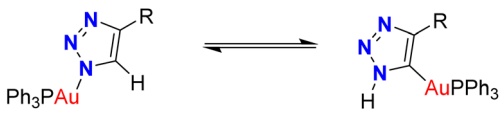

(1)

Complicating the composition of **7-H** and **8-H** further is that their ^{1}H NMR spectra reveal signals attributable to unreacted alkyne groups. For complex **7-H**, alkyne signals appear as three singlets between 3.48–2.91 ppm, and for the triazolate C–H proton, signals appear downfield between 9.22–8.34 ppm (page S29 in the ESI†). The multiple signals arise from the presence of two isomers noted above and the possibility of one and two unreacted alkynes. The ratio of the different branches within complex **7-H** as determined by NMR integration for C–H : N–H : C≡C–H is as follow: 0.07 : 0.64 : 0.29. For **8-H** the ratios is 0.42 : 0.46 : 0.12 (page S32 in the ESI†).

The FTIR spectra of all five model complexes (**7-AuPPh$_3$**, **7-AuPEt$_3$**, **8-AuPPh$_3$**, **7-H**, and **8-H**) do not contain an azide[54] signal near 2058 cm^{-1}, but a small absorption corresponding to unreacted alkyne[54] on the end groups at 2110 cm^{-1} supports the conclusion that in this case the iClick is not complete.

Synthesis of iClick network metallopolymers (5-AuPPh$_3$, 5-AuPEt$_3$, 5-H, 6-AuPPh$_3$, and 6-H)

Combining the digoldazido complex **2-AuN$_3$** with tri-goldacetylide **3-AuPPh$_3$** or **3-AuPEt$_3$**, tri-alkyne **3-H**, tetra-goldacetylide **4-AuPPh$_3$**, or tetra-alkyne **4-H** in CH_2Cl_2 yields five different iClick network metallopolymers (**5-AuPPh$_3$**, **5-AuPEt$_3$**, **5-H**, **6-AuPPh$_3$**, and **6-H**) according to Schemes 4 and 5. Table S1 in the ESI† summarizes the optimization of iClick network metallopolymer syntheses.

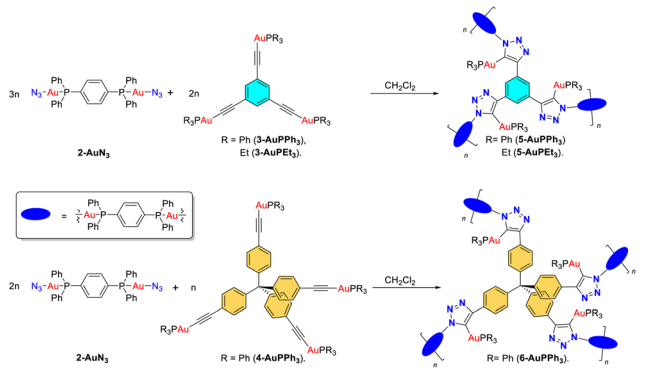

Scheme 4 Idealized structure of the iClick network metallopolymers (**5-AuPPh$_3$**, **5-AuPEt$_3$**, and **6-AuPPh$_3$**).

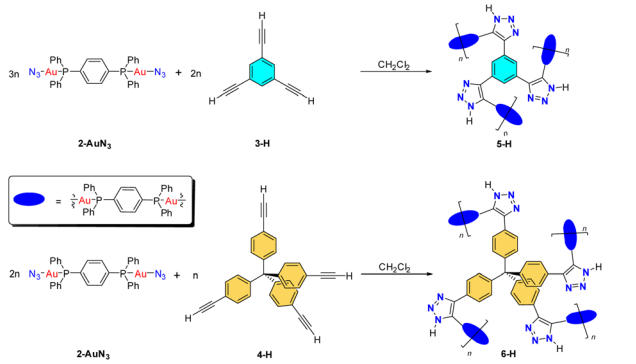

Scheme 5 Idealized structure of the iClick network metallopolymers (**5-H** and **6-H**).

Mixing a colorless solution of complex **2-AuN$_3$** with the light-yellow transparent gold(I) acetylide solution of **3-AuPPh$_3$**, **3-AuPEt$_3$**, or **4-AuPPh$_3$** in CH_2Cl_2 produces a light yellow suspension of network polymers **5-AuPPh$_3$**, **5-AuPEt$_3$**, or **6-AuPPh$_3$**, according to Scheme 4. Purification of the polymers involves simply filtering and washing with CH_2Cl_2. Other conditions attempted include continuous stirring at room temperature for 2 d, but the same yellow suspension forms (Table 1 entries **5-AuPPh$_3$-1** and **6-AuPPh$_3$-1**). Increasing the reaction temperature to 100 °C for 3 d yields brown solids with a colorless solution (Table 1 entries **5-AuPPh$_3$-3** and **6-AuPPh$_3$-3**). Heating at 50 °C for 6 d produces light pink network polymers **5-AuPPh$_3$**, **5-AuPEt$_3$**, and **6-AuPPh$_3$** that have the highest surface area (Table 1 entries **5-AuPPh$_3$-2**, **5-AuPEt$_3$**, and **6-AuPPh$_3$-2**).

It is also possible to produce network polymers using the organic tri- and tetra-alkynes **3-H** and **4-H** according to Scheme 5. Stirring the digoldazido complex **2-AuN$_3$** with trialkyne **3-H** in CH_2Cl_2 for 1 d at 50 °C results in a cream-colored suspension of **5-H** (Scheme 5). Table 1 entries **5-H-1** and **5-H-2** indicate that reaction time (1 d *vs.* 6 d) has negligible effect on the porosity outcome. Employing the same reaction conditions and workup produces network polymer **6-H** with similar surface areas.

Table 1 Effect of reaction time and reaction temperature on the pore properties of iClick network metallopolymers

iClick polymers	Entry	Reaction temp. (°C)	Reaction time (days)	Specific surface area[a] ($m^2\ g^{-1}$)
5-AuPPh$_3$	**5-AuPPh$_3$-1**	rt	2	27
	5-AuPPh$_3$-2	50	6	94
	5-AuPPh$_3$-3	100	3	54
6-AuPPh$_3$	**6-AuPPh$_3$-1**	rt	2	44
	6-AuPPh$_3$-2	50	6	85
	6-AuPPh$_3$-3	100	3	47
5-AuPEt$_3$	**5-AuPEt3**	50	6	30
5-H	**5-H-1**	50	1	28
	5-H-2	50	6	24
6-H	**6-H**	50	1	40

[a] BET specific surface area in the pressure range of 0.01–0.05 P/P_0 calculated using the BET model.

Examining the porosities of all polymers using nitrogen physisorption at 77 K reveals nitrogen adsorption and desorption isotherms that increase exponentially with increasing pressure indicative of type III isotherm (Fig. 3). Nonporous or macroporous solids display type III isotherms. Interestingly, only **6-AuPPh$_3$-2** exhibits a hysteresis loop desorption isotherm. Determined by N_2 adsorption–desorption isotherms, all five compounds exhibit surface areas below 100 $m^2\ g^{-1}$ (Table 1). Despite the low surface area, these compounds are the first iClick network metallopolymers that incorporate metal ions directly into the polymer scaffold. One reason for the low porosity maybe due to network collapse of the porous polymers, a common problem. Various synthetic procedures aimed at avoiding network collapse[93–95] failed to improve the surface area.

The FTIR and solid-state ^{13}C CPMAS NMR spectra confirm the formation of all five network polymers (**5-AuPPh$_3$-2**, **5-AuPEt$_3$**, **5-H-1**, **6-AuPPh$_3$-2**, and **6-H**). The FTIR spectra of the five polymers no longer exhibit the characteristic signal of the azide group (2052 cm^{-1}) though a small signal for the

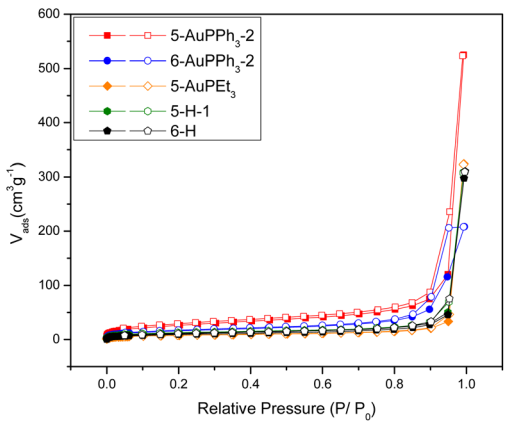

Fig. 3 N_2 adsorption–desorption isotherms of iClick network metallopolymers (**5Au-2**, **6Au-2**, **5AuPEt$_3$**, **5H-1**, and **6H**) (solid: adsorption; hollow: desorption).

unreacted gold(I) acetylide (2110 cm^{-1}) appears in all the materials. A new absorption at approximately 1584 cm^{-1} (NN stretch) is attributable to the formation of the expected triazolate ring (Fig. S34 in the ESI†).

The solid-state ^{13}C CPMAS NMR spectra of the network metallopolymers (**5-AuPPh$_3$-2**, **5-AuPEt$_3$**, **5-H-1**, **6-AuPPh$_3$-2**, and **6-H**) match well with the solid-state and solution-phase ^{13}C NMR spectra of the iClick model complexes (**7-AuPPh$_3$**, **7-AuPEt$_3$**, **8-AuPPh$_3$**, **7-H**, and **8-H**) (Fig. S35–S39†). The model complexes all demonstrate one or multiple signals from 150–160 ppm region that are attributable to the triazolate ring. The multiple signals are due to the partially unreacted click reaction, indicating model complex **8-AuPPh$_3$** has a mixture of mono-clicked, di-clicked, tri-clicked and fully-clicked arms. Similarly, the unreacted alkynes or acetylides exhibit multiple signals near 80 ppm. The NMR data of the model complexes mirrors the network polymers indicating successful iClick reactions.

Fig. 4A and B depicts the solid-state ^{13}C CPMAS NMR spectra of polymers **5-H-1** and **5-AuPPh$_3$-2**. **5-AuPPh$_3$-2** exhibits a resonance at 153.7 ppm that is attributable to the carbon on the triazolate ring and indicates a successful iClick reaction. A broad signal from 139.8–118.0 ppm corresponds to the aromatic carbons and a signal at 65.6 ppm is the unreacted gold(I)acetylides. Assigned to the carbon on the triazolate rings, two additional signals appear at 171.3 and 160.9 ppm, implying a mixture of expected isomers that were observed in complex **7-H** discussed above. The signals appearing at 82.3 and 77.1 ppm are unreacted alkynes that are also observed in model complexes and in the IR spectrum. The assignments match well with the solid-state and solution-phase ^{13}C NMR spectra of the model complexes **7-AuPPh$_3$** and **7-H** in Fig. S35 and S38.† Achieving 100% conversion within an insoluble polymer network is unlikely. Though not the subject of this study those remaining alkyne groups can serve as future sites for post-polymerization functionalization.

Both solid-state ^{13}C CPMAS NMR spectra of polymer **6-H** and **6-AuPPh$_3$-2** exhibit a broad signal from 139.0–122.3 assigned to the aromatic carbons on the polymer (Fig. 4C and D). The signal at 65.0 ppm belongs to the central aliphatic carbon of the linker. The triazolate ring carbons resonate at 160.3, 156.1, and 144.7 ppm. For polymer **6-AuPPh$_3$-2**, the appearance of these signals is due to the unreacted gold acetylides producing a mixture of mono-click, di-click, tri-click and fully-click complexes, which matches the solid-state ^{13}C NMR of the model complex in Fig. S36.† For polymer **6-H**, the three carbon signals are again attributable to the triazolate mixtures as discussed previously. Two additional alkyne signals at 81.1 and 68.3 ppm appear in the spectrum. Importantly, the solid-state ^{13}C CPMAS NMR spectra of all network polymers matches well with that of the solution-state $^{13}C\{^1H\}$ NMR of the model complexes, further supporting the assignments of the polymer structures (Fig. S35–S39 in the ESI†).

Thermogravimetric analysis (TGA) curves demonstrate that all polymers are thermally stable up to 290 °C (Fig. S40 in the ESI†). Polymer **5-AuPPh$_3$-2** and **6-AuPPh$_3$-2** depict a glass transition temperature (T_g) at −32.8 °C and −40.5 °C in the differential scanning calorimetry (DSC) data between −70 to 220 °C (Fig. S41 in the ESI†). Notably, the T_g and the absorption analysis are evidence of network polymers. Powder X-ray Diffraction (PXRD) data obtained for **5-AuPPh$_3$-2** and **6-AuPPh$_3$-2** confirm their amorphous composition (Fig. S53†). The TEM and STEM images of polymer **6-AuPPh$_3$-2** contains gold nanoparticles on the surface of the material as a minor impurity (confirmed by EDS). (Fig. S49 in the ESI†). The STEM EDS spectra demonstrates that the polymer **6-AuPPh$_3$-2** contains P and Au atoms, while the gold nanoparticles contain only Au (Fig. S51 in the ESI†).

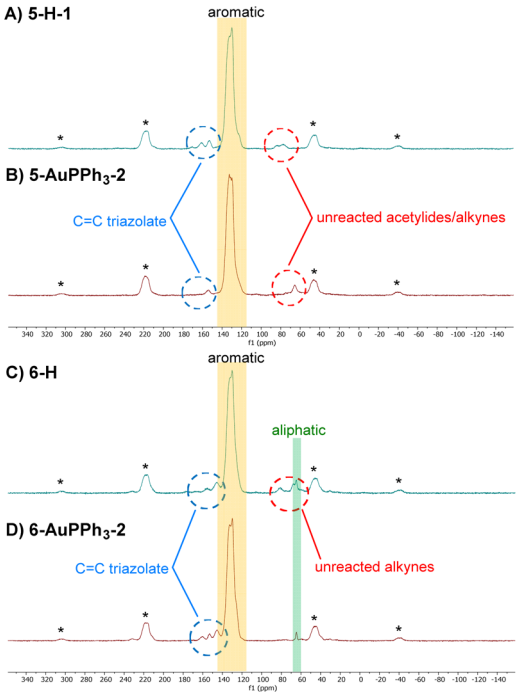

Fig. 4 The solid-state ^{13}C CPMAS NMR spectra of (A) **5-H-1**, (B) **5-AuPPh$_3$-2**, (C) **6-H**, and (D) **6-AuPPh$_3$-2** (* = spinning side bands (13 kHz)).

Discussion

Unreacted alkyne groups suggest the maximum degree of polymerization (DP) was not achieved during the iClick formation of these network polymers and may contribute to the low porosity. Another feature unique to this system that prevents high DP is that azide groups can undergo exchange and shunt polymer growth. Fig. 5 depicts the exchange reaction that eliminates an azide group from the monomer with free phosphine. Indeed, NMR studies indicate **2-AuN$_3$** rapidly exchanges with free phosphine. The $^{31}P\{^1H\}$ NMR spectrum of the mixture reveals a resonance attributable to PPh_3AuN_3 (**1-AuN$_3$**). Finally, bulky PPh_3 groups on the polymer branch also may account for the low surface area for all five complexes. The sterically hindered PPh_3 ligands could fill the pores preventing gas adsorption and resulting in type III isotherms.

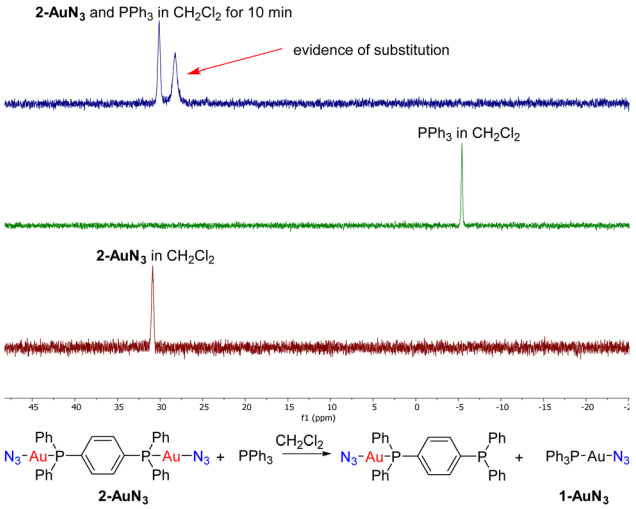

Fig. 5 (Top) Stacked $^{31}P\{^{1}H\}$ NMR spectra of an *in situ* experiment of adding **2-AuN$_3$** and **PPh$_3$** in CH_2Cl_2 for 10 min, PPh_3 in CH_2Cl_2, and **2-AuN$_3$** in CH_2Cl_2. (Bottom) Illustration of substitution reaction of **2-AuN$_3$** and PPh_3.

Polymers **5-H** and **6-H** have surface areas similar to **5-AuPPh$_3$-1** and **6-AuPPh$_3$-1**, indicating that for all four, the bulky PPh_3 ligands on the polymer backbone are filling the pores.

Investigating the CO_2 adsorption properties of all five polymers helps identify the different uptake capacities between the structures. Polymers **5-AuPPh$_3$-2**, **6-AuPPh$_3$-2**, and **6-H** all demonstrate CO_2 adsorption capacities of around 30 and 14 mg g^{-1} at 273 and 298 K, respectively (Table S4 in the ESI†). Judging from the higher surface areas of polymers **5-AuPPh$_3$-2** and **6-AuPPh$_3$-2**, it is obvious that both polymers demonstrate a higher CO_2 uptake amount.[54] The CO_2 adsorption capacities in **5-AuPEt$_3$** and **5-H-1** at 273 and 298 K are around 15 and 8 mg g^{-1} (Table S4 in the ESI†), respectively, which match the lower surface areas of the polymers. These results are lower in comparison to reported organic click-based polymers.[56,96]

Conclusion

Incorporating the digoldazido complex **2-AuN$_3$** with gold(I)acetylide or alkynes produces the first series of iClick network metallopolymers that are thermally stable and possess porous properties. This work expands the scope of metal containing porous polymers beyond the ligand classes of polypyridines, phthalocyanine, and porphyrins to now include triazolate ligands. The model complexes **7-AuPPh$_3$**, **7-AuPEt$_3$**, **8-AuPPh$_3$**, **7-H**, and **8-H** help elucidate the characterization features of the insoluble network polymers and revealed incomplete iClick reactions and triazolate isomerization. A measurable T_g, IR spectra showing the consumption of the azide/alkyne groups, solid-state ^{13}C NMR data confirming a triazolate within the material, and measurable surface areas, provide evidence supporting the assignment of iClick network polymers. Due to limited solubility, the degree of polymerization and extent of crosslinking remain to be interrogated. This study provides the beginnings of a new strategy to synthesize heterogeneous network metallopolymers with metals incorporated both within the main chain and side branches.

Conflicts of interest

There are no conflicts to declare.

Acknowledgements

Research supported by the U. S. Department of Energy, Office of Basic Energy Sciences, Division of Materials Sciences and Engineering under Award DE-SC0020008. The UF Mass Spectrometry Research and Education Center (NIH S10 OD021758-01A1) are thanked for acquisition of mass spectrometry data. K. A. A. acknowledges the NSF (CHE-1828064) for the purchase of X-ray equipment. Analytical data were obtained from the CENTC Elemental Analysis Facility at the University of Rochester, funded by NSF CHE-0650456. Solid-state NMR was performed in the McKnight Brain Institute at the National High Magnetic Field Laboratory's AMRIS Facility by Dr Anil Mehta and was supported by National Science Foundation cooperative agreement no. DMR-1644779 and the State of Florida. The NMR spectrometer used to acquire the solid-state NMR spectra was funded, in part, by an NIH award, S10 OD028753.

References

1 R. Schlögl, *Angew. Chem., Int. Ed.*, 2015, **54**, 3465–3520.
2 A. Corma and H. García, *Chem. Rev.*, 2003, **103**, 4307–4365.
3 Q. Sun, Z. Dai, X. Meng and F.-S. Xiao, *Chem. Soc. Rev.*, 2015, **44**, 6018–6034.
4 L. Tan and B. Tan, *Chem. Soc. Rev.*, 2017, **46**, 3322–3356.
5 Y. Xu, S. Jin, H. Xu, A. Nagai and D. Jiang, *Chem. Soc. Rev.*, 2013, **42**, 8012–8031.
6 T. Zhang, G. Xing, W. Chen and L. Chen, *Mater. Chem. Front.*, 2020, **4**, 332–353.
7 T.-X. Wang, H.-P. Liang, D. A. Anito, X. Ding and B.-H. Han, *J. Mater. Chem. A*, 2020, **8**, 7003–7034.
8 Y. Song, P. C. Lan, K. Martin and S. Ma, *Nanoscale Adv.*, 2021, **3**, 4891–4906.
9 M. Ateia, D. E. Helbling and W. R. Dichtel, *ACS Mater. Lett.*, 2020, **2**, 1532–1544.
10 Y. Zhang and S. N. Riduan, *Chem. Soc. Rev.*, 2012, **41**, 2083–2094.
11 L. Yang, J. Shui, L. Du, Y. Shao, J. Liu, L. Dai, Z. Hu, L. Yang, Z. Hu, J. Shui, L. Du, Y. Shao, J. Liu and L. Dai, *Adv. Mater.*, 2019, **31**, 1804799.
12 W. Zhang, J. J. Dynes, Y. Hu, P. Jiang and S. Ma, *Nat. Commun.*, 2019, **10**, 1–8.
13 Z. Li and Y.-W. Yang, *J. Mater. Chem. B*, 2017, **5**, 9278–9290.

14 P. Zhang, S. Wang, S. Ma, F. S. Xiao and Q. Sun, *Chem. Commun.*, 2020, **56**, 10631–10641.
15 S. Mondal, S. K. Kundu and A. Bhaumik, *Chem. Commun.*, 2017, **53**, 2752–2755.
16 X. Guo, E. Lin, J. Gao, T. Mao, D. Yan, P. Cheng, S. Ma, Y. Chen and Z. Zhang, *Angew. Chem., Int. Ed.*, 2021, **60**, 2974–2979.
17 R. Gomes, P. Bhanja and A. Bhaumik, *Chem. Commun.*, 2015, **51**, 10050–10053.
18 Y. Zhao, Y. Peng, C. Shan, Z. Lu, L. Wojtas, Z. Zhang, B. Zhang, Y. Feng and S. Ma, *Nano Res.*, 2021, **15**, 1145–1152.
19 Y. Song, Q. Sun, P. C. Lan and S. Ma, *ACS Appl. Mater. Interfaces*, 2020, **12**, 32827–32833.
20 M. L. Sun, Y. R. Wang, W. W. He, R. L. Zhong, Q. Z. Liu, S. Xu, J. M. Xu, X. L. Han, X. Ge, S. L. Li, Y. Q. Lan, A. M. Al-Enizi, A. Nafady and S. Ma, *Small*, 2021, **17**, 2100762.
21 K. Huang, J. Y. Zhang, F. Liu and S. Dai, *ACS Catal.*, 2018, **8**, 9079–9102.
22 Q. Sun, B. Aguila, Y. Song and S. Ma, *Acc. Chem. Res.*, 2020, **53**, 812–821.
23 B. Aguila, Q. Sun, H. C. Cassady, C. Shan, Z. Liang, A. M. Al-Enizic, A. Nafadyc, J. T. Wright, R. W. Meulenberg, S. Ma, B. Aguila, H. C. Cassady, C. Shan, S. Ma, Q. Sun, Z. Liang, A. M. Al-Enizic, A. Nafadyc, J. T. Wright and R. W. Meulenberg, *Angew. Chem., Int. Ed.*, 2020, **59**, 19618–19622.
24 Y. Zhang, B. Aguila, S. Ma and Q. Zhang, *J. Environ. Chem. Eng.*, 2020, **8**, 104296.
25 L. Hou, C. Shan, Y. Song, S. Chen, L. Wojtas, S. Ma, Q. Sun and L. Zhang, *Angew. Chem., Int. Ed.*, 2021, **60**, 14664–14670.
26 Y. Ling, D. M. Alzate-Sánchez, M. J. Klemes, W. R. Dichtel and D. E. Helbling, *Water Res.*, 2020, **173**, 115551–115561.
27 C. Wu, M. J. Klemes, B. Trang, W. R. Dichtel and D. E. Helbling, *Water Res.*, 2020, **182**, 115950–115959.
28 C. Ching, M. J. Klemes, B. Trang, W. R. Dichtel and D. E. Helbling, *Environ. Sci. Technol.*, 2020, **54**, 12693–12702.
29 L. Xiao, C. Ching, Y. Ling, M. Nasiri, M. J. Klemes, T. M. Reineke, D. E. Helbling and W. R. Dichtel, *Macromolecules*, 2019, **52**, 3747–3752.
30 S. Kramer, N. R. Bennedsen and S. Kegnæs, *ACS Catal.*, 2018, **8**, 6961–6982.
31 H.-P. Liang, A. Acharjya, D. A. Anito, S. Vogl, T.-X. Wang, A. Thomas and B.-H. Han, *ACS Catal.*, 2019, **9**, 3959–3968.
32 M. Liras, M. Pintado-Sierra, M. Iglesias and F. Sánchez, *J. Mater. Chem. A*, 2016, **4**, 17274–17278.
33 W. Liang, T. L. Church, S. Zheng, C. Zhou, B. S. Haynes and D. M. D'Alessandro, *Chem. – Eur. J.*, 2015, **21**, 18576–18579.
34 X. Ding and B.-H. Han, *Angew. Chem., Int. Ed.*, 2015, **54**, 6536–6539.
35 W.-L. He and C.-D. Wu, *Appl. Catal., B*, 2018, **234**, 290–295.
36 K. Zhang, O. K. Farha, J. T. Hupp and S. T. Nguyen, *ACS Catal.*, 2015, **5**, 4859–4866.
37 S. Meng, X. Zou, C. Liu, H. Ma, N. Zhao, H. Ren, M. Jia, J. Liu and G. Zhu, *ChemCatChem*, 2016, **8**, 2393–2400.
38 H.-P. Liang, Q. Chen and B.-H. Han, *ACS Catal.*, 2018, **8**, 5313–5322.
39 L. Pan, M.-Y. Xu, L.-J. Feng, Q. Chen, Y.-J. He and B.-H. Han, *Polym. Chem.*, 2016, **7**, 2299–2307.
40 J.-L. Wang, C. Wang, K. E. deKrafft and W. Lin, *ACS Catal.*, 2012, **2**, 417–424.
41 Z. Xie, C. Wang, K. E. deKrafft and W. Lin, *J. Am. Chem. Soc.*, 2011, **133**, 2056–2059.
42 K. Cho, H.-S. Yang, I.-H. Lee, S. M. Lee, H. J. Kim and S. U. Son, *J. Am. Chem. Soc.*, 2021, **143**, 4100–4106.
43 Z. J. Wang, R. Li, K. Landfester and K. A. I. Zhang, *Polymer*, 2017, **126**, 291–295.
44 T. Ben, H. Ren, S. Ma, D. Cao, J. Lan, X. Jing, W. Wang, J. Xu, F. Deng, J. M. Simmons, S. Qiu and G. Zhu, *Angew. Chem., Int. Ed.*, 2009, **48**, 9457–9460.
45 B. Li, Y. Zhang, D. Ma, Z. Shi and S. Ma, *Nat. Commun.*, 2014, **5**, 1–7.
46 B. G. Hauser, O. K. Farha, J. Exley and J. T. Hupp, *Chem. Mater.*, 2013, **25**, 12–16.
47 J.-X. Jiang, F. Su, A. Trewin, C. D. Wood, N. L. Campbell, H. Niu, C. Dickinson, A. Y. Ganin, M. J. Rosseinsky, Y. Z. Khimyak and A. I. Cooper, *Angew. Chem., Int. Ed.*, 2007, **46**, 8574–8578.
48 L. Chen, Y. Yang and D. Jiang, *J. Am. Chem. Soc.*, 2010, **132**, 9138–9143.
49 J. Germain, J. Hradil, J. M. J. Fréchet and F. Svec, *Chem. Mater.*, 2006, **18**, 4430–4435.
50 Z. A. Qiao, S. H. Chai, K. Nelson, Z. Bi, J. Chen, S. M. Mahurin, X. Zhu and S. Dai, *Nat. Commun.*, 2014, **5**, 1–8.
51 B. Li, Z. Guan, W. Wang, X. Yang, J. Hu, B. Tan and T. Li, *Adv. Mater.*, 2012, **24**, 3390–3395.
52 L. Li, H. Zhao, J. Wang and R. Wang, *ACS Nano*, 2014, **8**, 5352–5364.
53 J. R. Holst, E. Stöckel, D. J. Adams and A. I. Cooper, *Macromolecules*, 2010, **43**, 8531–8538.
54 P. Pandey, O. K. Farha, A. M. Spokoyny, C. A. Mirkin, M. G. Kanatzidis, J. T. Hupp and S. T. Nguyen, *J. Mater. Chem.*, 2011, **21**, 1700–1703.
55 S. Mukherjee, M. Das, A. Manna, R. Krishna and S. Das, *J. Mater. Chem. A*, 2019, **7**, 1055–1068.
56 C. Cui, R. Sa, Z. Hong, H. Zhong and R. Wang, *ChemSusChem*, 2020, **13**, 180–187.
57 S. Mukherjee, M. Das, A. Manna, R. Krishna and S. Das, *Chem. Mater.*, 2019, **31**, 3929–3940.
58 L.-H. Xie and M. P. Suh, *Chem. – Eur. J.*, 2013, **19**, 11590–11597.
59 R. Bera, M. Ansari, S. Mondal and N. Das, *Eur. Polym. J.*, 2018, **99**, 259–267.
60 O. Plietzsch, C. I. Schilling, T. Grab, S. L. Grage, A. S. Ulrich, A. Comotti, P. Sozzani, T. Muller and S. Bräse, *New J. Chem.*, 2011, **35**, 1577–1581.

61 F. Wei, X. Cai, J. Nie, F. Wang, C. Lu, G. Yang, Z. Chen, C. Ma and Y. Zhang, *Polym. Chem.*, 2018, **9**, 3832–3839.
62 C. Song, J. Nie, C. Ma, C. Lu, F. Wang and G. Yang, *Appl. Catal., B*, 2021, **287**, 119984–119995.
63 L. Li, C. Zhou, H. Zhao and R. Wang, *Nano Res.*, 2015, **8**, 709–721.
64 T. J. Del Castillo, S. Sarkar, K. A. Abboud and A. S. Veige, *Dalton Trans.*, 2011, **40**, 8140–8144.
65 X. Yang, S. VenkatRamani, C. C. Beto, T. J. Del Castillo, I. Ghiviriga, K. A. Abboud and A. S. Veige, *Organometallics*, 2017, **36**, 1352–1357.
66 C. C. Beto, Y. Yang, C. J. Zeman, I. Ghiviriga, K. S. Schanze and A. S. Veige, *Organometallics*, 2018, **37**, 4545–4550.
67 C. C. Beto, E. D. Holt, Y. Yang, I. Ghiviriga, K. S. Schanze and A. S. Veige, *Chem. Commun.*, 2017, **53**, 9934–9937.
68 D. V. Partyka, J. B. U. I. Updegraff III, M. Zeller, A. D. Hunter and T. G. Gray, *Organometallics*, 2006, **26**, 183–186.
69 W. P. Fehlhammer and W. Beck, *Z. Anorg. Allg. Chem.*, 2015, **641**, 1599–1678.
70 H. W. Frühauf, *Chem. Rev.*, 1997, **97**, 523–596.
71 P. V. Simpson, B. W. Skelton, P. Raiteri and M. Massi, *New J. Chem.*, 2016, **40**, 5797–5807.
72 P. Schmid, M. Maier, H. Pfeiffer, A. Belz, L. Henry, A. Friedrich, F. Schönfeld, K. Edkins and U. Schatzschneider, *Dalton Trans.*, 2017, **46**, 13386–13396.
73 A. Rosan and M. Rosenblum, *J. Organomet. Chem.*, 1974, **80**, 103–107.
74 T. Daniel, W. Knaup, M. Dziallas and H. Werner, *Chem. Ber.*, 1993, **126**, 1981–1993.
75 D. V. Partyka, J. B. Updegraff, M. Zeller, A. D. Hunter and T. G. Gray, *Organometallics*, 2007, **26**, 183–186.
76 N. J. Farrer and D. M. Griffith, *Curr. Opin. Chem. Biol.*, 2020, **55**, 59–68.
77 Y. H. Shen, A. M. Esper, I. Ghiviriga, K. A. Abboud, K. S. Schanze, C. Ehm and A. S. Veige, *Dalton Trans.*, 2021, **50**, 12681–12691.
78 K. Peng, V. Mawamba, E. Schulz, M. Löhr, C. Hagemann and U. Schatzschneider, *Inorg. Chem.*, 2019, **58**, 11508–11521.
79 L. Waag-Hiersch, J. Mößeler and U. Schatzschneider, *Eur. J. Inorg. Chem.*, 2017, **2017**, 3024–3029.
80 L. Henry, C. Schneider, B. Mützel, P. V. Simpson, C. Nagel, K. Fucke and U. Schatzschneider, *Chem. Commun.*, 2014, **50**, 15692–15695.
81 A. R. Powers, X. Yang, T. J. Del Castillo, I. Ghiviriga, K. A. Abboud and A. S. Veige, *Dalton Trans.*, 2013, **42**, 14963–14966.
82 C. J. Zeman, Y. H. Shen, J. K. Heller, K. A. Abboud, K. S. Schanze and A. S. Veige, *J. Am. Chem. Soc.*, 2020, **142**, 8331–8341.
83 X. Yang, S. Wang, I. Ghiviriga, K. A. Abboud and A. S. Veige, *Dalton Trans.*, 2015, **44**, 11437–11443.
84 A. R. Powers, I. Ghiviriga, K. A. Abboud and A. S. Veige, *Dalton Trans.*, 2015, **44**, 14747–14752.
85 C. C. Beto, X. Yang, A. R. Powers, I. Ghiviriga, K. A. Abboud and A. S. Veige, *Polyhedron*, 2016, **108**, 87–92.
86 C. C. Beto, E. D. Holt, Y. Yang, I. Ghiviriga, K. S. Schanze and A. S. Veige, *Chem. Commun.*, 2017, **53**, 9934–9937.
87 C. C. Beto, I. Charles, J. Zeman, Y. Yang, J. D. Bullock, E. D. Holt, A. Q. Kane, T. A. Makal, X. Yang, I. Ghiviriga, K. S. Schanze and A. S. Veige, *Inorg. Chem.*, 2020, **59**, 1893–1904.
88 J. Cámara, O. Crespo, M. C. Gimeno, I. O. Koshevoy, A. Laguna, I. Ospino, E. S. Smirnova and S. P. Tunik, *Dalton Trans.*, 2012, **41**, 13891–13898.
89 I. R. Whittall, M. G. Humphrey, S. Houbrechts, J. Maes, A. Persoons, S. Schmid and D. C. R. Hockless, *J. Organomet. Chem.*, 1997, **544**, 277–283.
90 J. Luo, X. Liu, M. Ma, J. Tang and F. Huang, *Eur. Polym. J.*, 2020, **129**, 109628.
91 H. C. Kolb, M. G. Finn and K. B. Sharpless, *Angew. Chem., Int. Ed.*, 2001, **40**, 2004–2021.
92 T. Nakano, *Polym. J.*, 2010, **42**, 103–123.
93 E. Vitaku and W. R. Dichtel, *J. Am. Chem. Soc.*, 2017, **139**, 12911–12914.
94 D. Zhu and R. Verduzco, *ACS Appl. Mater. Interfaces*, 2020, **12**, 33121–33127.
95 C. H. Feriante, S. Jhulki, A. M. Evans, R. R. Dasari, K. Slicker, W. R. Dichtel, S. R. Marder, C. H. Feriante, S. Jhulki, R. R. Dasari, K. Slicker, S. R. Marder, A. M. Evans and W. R. Dichtel, *Adv. Mater.*, 2020, **32**, 1905776.
96 L. Li, H. Zhao and R. Wang, *ACS Catal.*, 2015, **5**, 948–955.